Available online at www.sciencedirect.com
SCIENCE DIRECT®
Journal of Solid State Chemistry 177 (2004) 268–273
JOURNAL OF SOLID STATE CHEMISTRY
http://elsevier.com/locate/jssc

Crystal growth and structure of a new manganese vanado-antimonate $MnVSbO_6$

L. Rambert,[a] P. Bordet,[a] A. Sulpice,[b] and P. Strobel[a,*]

[a] *Laboratoire de Cristallographie CNRS, BP 166X, 38042 Grenoble Cedex 9, France*
[b] *Centre de Recherches sur les très basses températures, CNRS, BP 166X, 38042 Grenoble Cedex 9, France*

Received 21 February 2003; received in revised form 4 June 2003; accepted 8 August 2003

Abstract

Single crystals of a new compound of formula $MnVSbO_6$ were grown by slow cooling from a V_2O_5–B_2O3_3 flux at 900°C. The compound crystallizes in the orthorhombic space group *Pbcn* (No. 60), with cell parameters (in the *Pcnb* setting) $a = 4.6604(3)$ Å, $b = 4.9603(3)$ Å, $c = 17.1433(9)$Å, $Z = 4$. The crystal structure was solved from 1188 independent reflections to $R_w = 3.20\%$ and goodness-of-fit 1.5 for 44 refined parameters. The structure can be described as a superstructure of the α-PbO_2 type with a cation ordering similar to that found in Fe_2WO_6. Cations occupy octahedral sites in the PbO_2-like layers. Zigzag chains of edge-sharing MnO_6 octahedra alternate with mixed Sb/V chains following a –Mn–Sb/V–Sb/V– sequence. The magnetic susceptibility of $MnVSbO_6$ follows the Curie–Weiss law down to ca. 15 K, where it orders antiferromagnetically. The bond lengths and Curie constant are consistent with the expected charge distribution $Mn^{2+}V^{5+}Sb^{5+}O_6$.

Keywords: Manganese-vanadium-antimony oxide; Crystal structure

1. Introduction

The Mn–Sb–O system contains a limited number of known compounds, namely $MnSb_2O_4$ and $Mn_3Sb_2O_6$ (JCPDS card 20-702), with trivalent antimony, $MnSb_2O_6$ and $Mn_2Sb_2O_7$ with pentavalent antimony. In the latter case, several peculiarities can be noted: $MnSb_2O_6$ (reported to crystallize with a columbite or trirutile structure in the early literature) is the only 1:2:6 antimonate with a Na_2SiF_6-related structure [1], while $Mn_2Sb_2O_7$ also adopts a structure different from that of other $M_2Sb_2O_7$ with weberite or pyrochlore structure when synthesized at high-temperature [2]. This is all the more surprising that pyrochlore-type oxides containing Mn^{2+} and Sb^{5+} are well known, as the oxygen-deficient series $(R\mathrm{Mn})(\mathrm{MnSb})O_3$ (R = rare earth) [3,4]. According to Brisse et al., pyrochlore-type $Mn_2Sb_2O_7$ is only stable at temperatures <600°C [5].

Reports about crystal growth in the Mn–Sb–O system are also scarce. V_2O_5 has been extensively used as a flux component for the crystal growth of various ternary oxides, often in association with B_2O_3, PbO or Bi_2O_3 [6]. However, very few of the oxides grown from such fluxes contained both transition-metal and an element of the group As–Sb–Bi [6–8]. Nakua and Greedan reported the growth of various MSb_2O_6 oxides from a V_2O_5 flux, including $MnSb_2O_6$ [9]. During attempts of crystal growth of other Mn–Sb–O phases from this flux, mm-size crystals of a new phase with formula $MnVSbO_6$ were obtained. This paper reports the crystal growth, X-ray structure determination and magnetic susceptibility of this new phase.

2. Experimental

Flux growth experiments were carried out in a 50 mL platinum crucible, using a V_2O_5 flux. As reported in Ref. [5], a fraction of B_2O_3 (9.6 wt%) was added to the V_2O_5 flux in order to improve its dissolving power. Starting materials were reagent grade Sb_2O_5, $Mn(CH_3COO)_2 \cdot 4H_2O$ or $MnCO_3$, V_2O_5 and anhydrous B_2O_3 (Aldrich). The charge/flux weight ratio was 0.20 and the total mass used in each attempt was 25–40 g. Detailed heating/cooling conditions are given in Table 1. At the final

*Corresponding author. Fax: +33-476-88-7940.
E-mail address: strobel@polycnrs-gre.fr (P. Strobel).

0022-4596/$ - see front matter © 2003 Elsevier Inc. All rights reserved.
doi:10.1016/j.jssc.2003.08.009

Table 1
Selected examples of crystal growth conditions

Run	Initial Mn/Sb ratio (atomic)	Flux	Soaking conditions	Cooling rate (°C/h)	Final temperature (°C)	Crystals formed
Ref. [5]	0.5	V_2O_5–B_2O_3	1000°C, 5 h	5	650	$MnSb_2O_6$
#5	1	V_2O_5–B_2O_3	950°C, 4 h	2.5	725	$MnSb_2O_6$
#9	3	V_2O_5–B_2O_3	900°C, 3 h	1.5	700	$MnVSbO_6$
#18	12	KCl–$MnCl_2$	900°C, 10 h	3	600	Mn_2O_3

temperature of the growth program, the flux was hot-poured on a steel plate and washed away in diluted hydrochloric acid. Crystals were recovered from both the poured flux fraction and the bottom of the crucible.

In an attempt to reach Mn-richer compounds, an additional run was carried out using a KCl–$MnCl_2$ flux with a composition close to the eutectic (2:1). Chloride-based flux have been used previously in the crystal growth of various ternary manganese oxides with lithium [10–12], calcium [13] or germanium [14] as third constituant.

Crystals were examined using a JEOL 800 scanning electron microscope equipped with a Kevex energy-dispersive X-ray emission analyzer. Preliminary phase identification was carried out by X-ray powder diffraction with crushed crystals on a Bruker D-5000 diffractometer in transmission geometry.

For crystal structure determination, a rectangle-shaped crystal of dimensions $320 \times 198 \times 35\,\mu m$ was selected and used for X-ray diffraction data collection using a Nonius Kappa CCD diffractometer. The Ag$K\alpha$ radiation ($\lambda = 0.5608$ Å) selected with a graphite monochromator was used. After determination of the crystal orientation matrix, diffraction data were collected with the rotation technique by measuring two omega scans comprising 223 frames of 1.3° oscillation angle with 13 s exposure time per frame. The sample to detector distance was set to 40 mm, and the maximum theta angle was 30°, leading to a resolution limit of $\sin\theta/\lambda \approx 0.9$ Å^{-1}. Diffracted intensities were extracted with the Denzo-SMN software [15]. The Maxus suite [16] was used for data analysis and structure solution. An absorption correction was applied using the description of the crystal faces by the gaussian integration technique [17] ($Z = 4$, $\mu = 49.82\,cm^{-1}$, $T_{min} = 0.3713$, $T_{max} = 0.7978$). The structure was solved by direct methods with SIR92 [18], which gave all atomic positions with a 6.4% R factor using default settings. Equivalent reflexion averaging and structure refinements were carried out with the Jana2000 program [19].

Magnetic measurements were carried out in a commercial Squid magnetometer. The field was applied perpendicular to c with an accuracy of a few degrees. The sample was cooled in zero field, then the field was applied at 4.2 K and the magnetization was measured on increasing (ZFC) and decreasing (FC) temperature in the range 4.2–300 K. The applied magnetic field was 100 Oe.

3. Results and discussion

3.1. Crystal growth

The main results of crystal growth experiments are summarized in Table 1. Contrary to expectations, using a Mn/Sb ratio = 1 (run 5) did not yield the desired $Mn_2Sb_2O_7$ phase, but gave $MnSb_2O_6$, i.e. the same phase as that grown previously using a Mn/Sb = 0.5 stoichiometry ratio [5]. Increasing the Mn/Sb ratio did not yield $Mn_2Sb_2O_7$ either, but a new vanadium-containing phase $MnVSbO_6$, as established from EDX analysis. The last attempt using a Mn-rich flux did not yield any antimony-containing compound, but the manganese oxide stable in the temperature range used, i.e. Mn_2O_3. The growth of a composition such as $Mn_2Sb_2O_7$ is probably hindered by a too large solubility difference between antimony and manganese in molten V_2O_5.

The morphology of crystals is illustrated in Fig. 1. $MnSb_2O_6$ crystals appear as black plates with a clear hexagonal habit (Fig. 1a). $MnVSbO_6$ crystals are black, shiny parallelipeds up to 1 mm in edge.

3.2. Crystal structure analysis

Data collection up to maximum theta 30° yielded 5528 diffracted intensities. The refined cell parameters obtained from the positions of these reflexions were $a = 4.6604(3)$ Å, $b = 4.9603(3)$ Å, $c = 17.1433(9)$ Å. Inspection of the systematic absences lead to the choice of space group *Pcnb*, which is an unconventional setting of *Pbcn* (#60). The absorption-corrected intensities were averaged in point group *mmm*, leading to 1188 independent reflexions with $R_{int} = 5.09$. The refinement was carried out on F values with all measured reflexions and statistical weights. The final cycles included anisotropic atomic displacement parameters for all atoms and an isotropic extinction correction of type I, lorentzian distribution (giso = 0.029(8)), and yielded agreement factors $R = 3.57\%$, $R_w = 3.20\%$ and GOF = 1.5 for 44 refined parameters. The refined

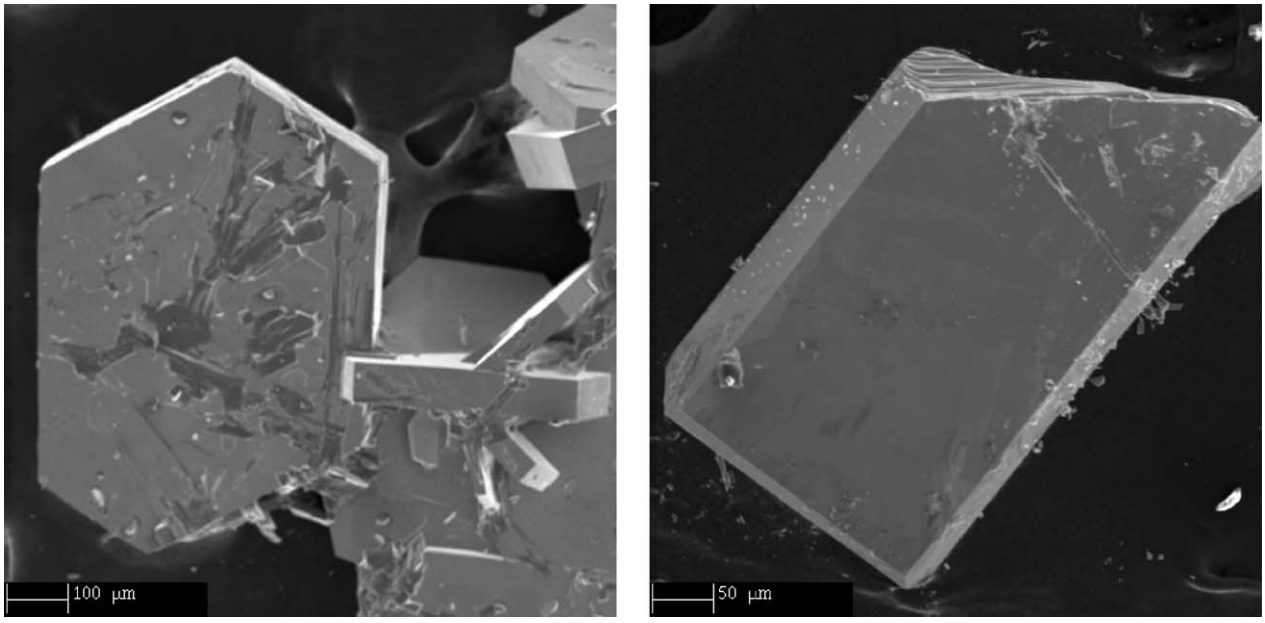

(a) (b)

Fig. 1. SEM pictures of single crystals of $MnSb_2O_6$ (a) and $MnVSbO_6$ (b).

Table 2
Atomic positions and displacement parameters for $SbMnVO_6$, space group *Pcnb* (#60), $a = 4.6604(3)$ Å, $b = 4.9603(3)$ Å, $c = 17.1433(9)$ Å

Atom	pos.	x	y	z	U_{11}	U_{22}	U_{33}	U_{12}	
Sb	4*c*	0	0.25	0.78082(1)	0.00401(9)	0.00341(9)	0.0042(1)	0.00031(5)	0
Mn	4*c*	0.5	0.25	0.93896(3)	0.0052(2)	0.0058(2)	0.0064(2)	−0.00088(1)	0
V	4*c*	0	0.75	0.89690(3)	0.0034(2)	0.0028(2)	0.0038(2)	−0.0001(1)	0
O1	8*d*	0.2036(2)	0.0589(3)	0.86587(9)	0.0055(5)	0.0047(4)	0.0053(5)	−0.0013(4)	−0.0
O2	8*d*	0.2466(3)	0.6150(3)	0.95691(9)	0.0072(6)	0.0064(5)	0.0074(5)	0.0004(4)	−0.0
O3	8*d*	0.2547(3)	0.0747(3)	0.70536(9)	0.0068(5)	0.0044(4)	0.0058(5)	0.0028(4)	0.0

structural parameters and principal interatomic distances are given in Tables 2 and 3.

The structure is represented in Fig. 2. It can be described as a superstructure of the α-PbO_2 type structure. In the latter, oxygen anions form a hexagonal close packed (hcp) network with half of the octahedral sites occupied by Pb^{4+} cations. These PbO_6 octahedra share edges to form zigzag chains along the *c*-axis. Layers perpendicular to the hcp stacking axis (the *a*-axis) are formed by alternating empty and full zigzag chains, as shown in Fig. 3a. The PbO_6 octahedra of adjacent layers are connected via corner sharing. This arrangement can lead to various types of superstructures, having different cation ordering schemes. For example, the columbite structure ($FeNb_2O_6$), contains cation layers alternating along the hcp stacking axis following a –Fe–Nb–Nb– sequence [20]. In Fe_2WO_6 [21], cation ordering takes place within each layer. As shown in Fig. 3b, chains of Fe octahedra order with

Table 3
Cation–anion distances, average distances and cation valences calculated by the bond valence sum method for $SbMnVO_6$

	Distance	Bond valence
Mn–O1 × 2	2.092(1)	0.442
Mn–O2 × 2	2.184(1)	0.345
Mn–O2 × 2	2.243(1)	0.294
Average (sigma)	2.173(0.076)	
v(Mn)		2.16
Sb–O1 × 2	1.982(1)	0.898
Sb–O3 × 2	1.960(1)	0.953
Sb–O3 × 2	1.990(1)	0.878
Average (sigma)	1.977(0.016)	
v(Sb)		5.46
V–O1 × 2	1.880(1)	0.812
V–O2 × 2	1.682(1)	1.387
V–O3 × 2	2.267(1)	0.285
Average (sigma)	1.943(0.298)	
v(V)		4.97

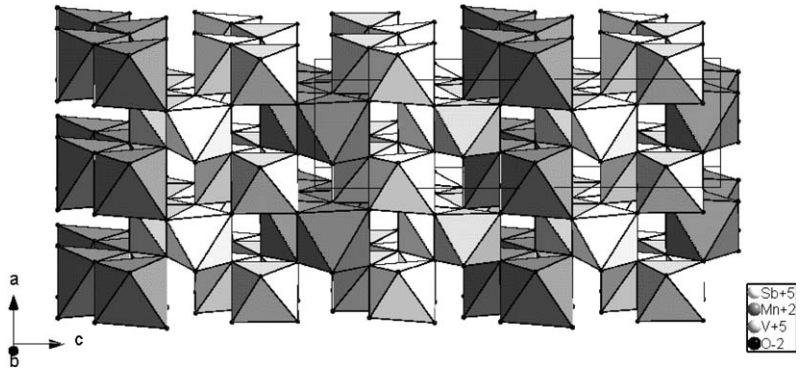

Fig. 2. Representation of the $MnVSbO_6$ structure. Dark gray octahedra contain Mn^{2+} cations, medium gray V^{5+} and light gray Sb^{5+}.

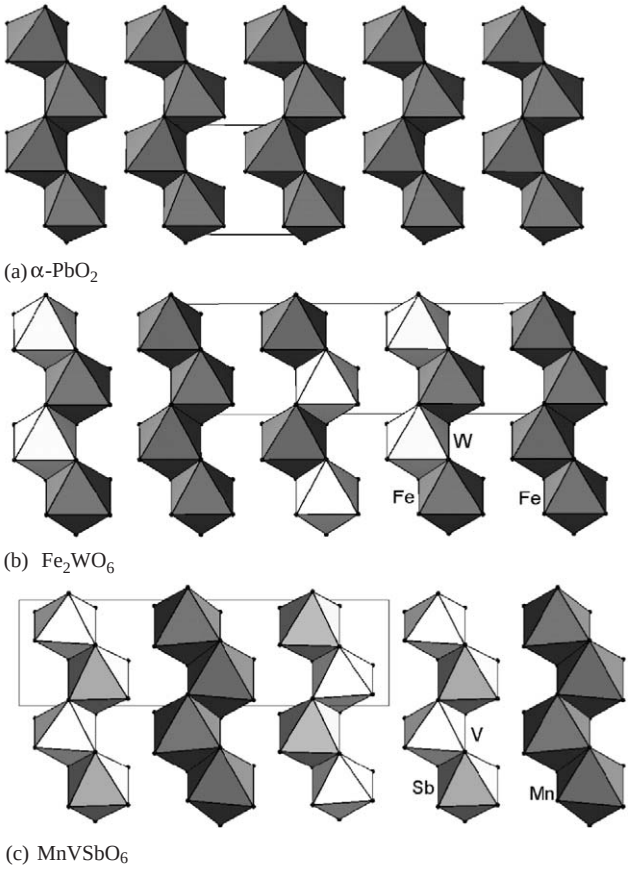

(a) α-PbO_2

(b) Fe_2WO_6

(c) $MnVSbO_6$

Fig. 3. Comparison of the crystal structures of α-PbO_2 (a), Fe_2WO_6 (b) and $MnVSbO_6$ (c).

chains of alternating Fe and W octahedral, following a –Fe–(Fe/W)–(Fe/W)– chain sequence perpendicular to the chain direction. In each mixed chain, Fe and W cations alternate along the chain direction. $MnVSbO_6$ is isostructural with the latter compound. In each α-PbO_2-like layer, zigzag chains of edge-sharing MnO_6 octahedra order with chains of alternating Sb and V octahedral, following a –Mn–Sb/V–Sb/V– chain sequence perpendicular to the chain direction (Fig. 3c). This arrangement leads to a considerable distortion with respect to a regular hcp network, driven by the requirement to accommodate cations with rather different ionic radii (Mn^{2+} [high spin]: 0.83 Å, Sb^{5+}: 0.60 Å and V^{5+}: 0.54 Å [22]). The average Mn–O distance observed (2.17 Å) is in good agreement with high spin Mn^{2+}.

The large cation size difference probably prevents the formation of a columbite-like superstructure containing layers with a single type of cation. In addition, chains formed by the large Mn^{2+} cations are separated from those where the smaller V^{5+} and Sb^{5+} are mixed. As seen in Table 3, the valences calculated by the bond valence sum technique [23], for the Mn^{2+} and V^{5+} cations agree well with the expected values, while the Sb^{5+} cation appears to be in a compressed state. Moreover, the formation of the chains by edge sharing brings about local distortions of the octahedra. In each coordination octahedron, four of the six oxygen anions belong to edges which are shared with an adjacent octahedron of the same chain. The cations tend to move towards the edge formed by the remaining two oxygen anions, in order to increase the cation–cation distances across the shared edges (see figure). This effect is particularly obvious for the V^{5+} cation, which is strongly displaced from the center of its coordination polyhedron towards the edge formed by two O_2 anions, with very short V–O distances of 1.68 Å. This also leads to a deformation of the polyhedron itself: in the case of the VO_6 octahedron, for instance, O–O distances range from 2.51 Å (for the shared edges) to 2.79 Å.

3.3. Magnetic susceptibility

The inverse magnetic susceptibility of $MnSbVO_6$ is shown in Figs. 4 and 5. No significant discrepancies were observed between FC and ZFC measurements. It follows the Curie–Weiss law down to ca. 15 K, then shows an upturn (see also inset in Fig. 4), which may indicate either antiferromagnetic ordering or at least some two-dimensional ordering. The Curie–Weiss parameters have been extracted by a linear fit, yielding

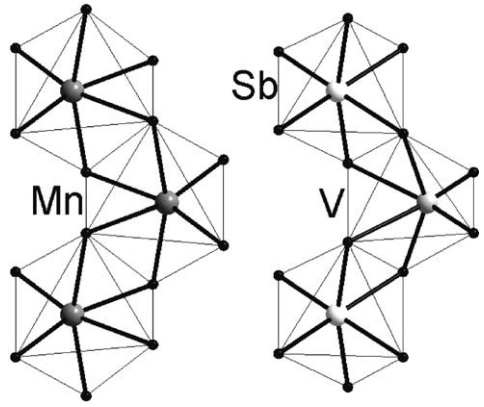

Fig. 4. *a*-axis projection of Mn and Sb/V zigzag chain fragments showing the displacement of the cations from the center of their coordination octahedra towards an unshared edge.

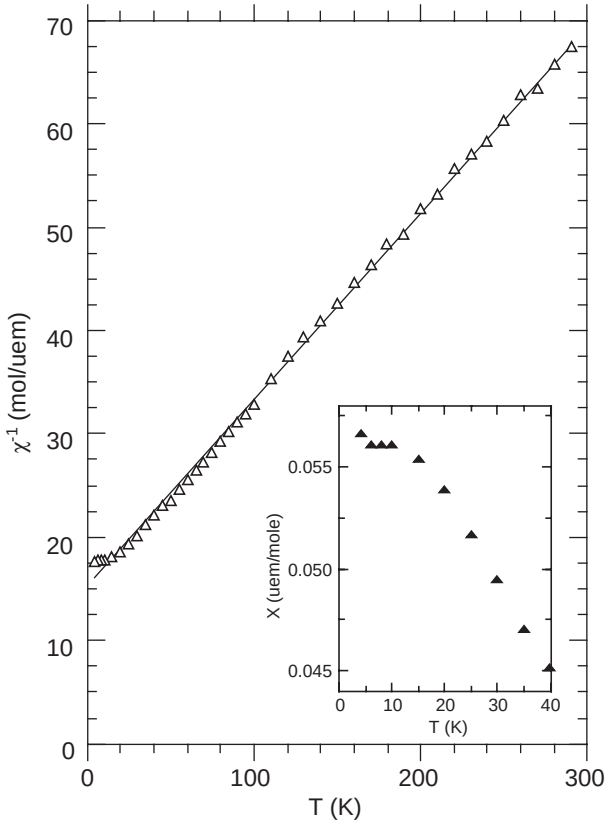

Fig. 5. Temperature dependence of the reciprocal magnetic susceptibility, measured in a field of 100 Oe.

$C = 5.53$ and $\Theta \approx -80$ K. The Curie constant gives a magnetic moment of $6.65\mu_B$, in fairly good agreement with the theoretical value expected ($5.92\mu_B$) for high-spin Mn^{2+} ($S = \frac{5}{2}$); note that the small mass of the sample used led to an uncertainty of ca. 5% on the magnetic susceptibility.

The experimental Weiss constant Θ is in agreement with dominant antiferromagnetic interactions. The zigzag manganese chains in $MnSbVO_6$ provide a rather simple topology of the manganese network. Each Mn ion has two Mn neighbors at 3.2 Å in the chain, with Mn–O–Mn angles 94.3°. This geometry presents some similarity with that in $MnSb_2O_6$, for instance, which contains chains of Mn^{2+} ions and orders antiferromagnetically at ≈ 12.5 K [1]. In $MnSbVO_6$, however, Mn neighbors in adjacent chains are much farther apart (4.6 Å), and no significant deviation from the Curie–Weiss law is observed above T_N, whereas $MnSb_2O_6$, with a more pronounced two-dimension character, exhibits a strong deviation from the Curie–Weiss behavior below 200 K.

4. Conclusions

Single crystals of a new ordered oxide $MnVSbO_6$ were obtained by a flux growth technique, using a higher Mn/Sb ratio than that used to produce $MnSb_2O_6$. The crystal structure of the new phase was determined, and corresponds to one of the numerous ordered variants of the α-PbO_2 structure type. The occurrence of such a α-PbO_2 superstructure is consistent with the rather large differences in size between the cations present in this compound. Susceptibility measurements showed evidence of an antiferromagnetic behavior at low temperature (<15 K), with no significant deviation from the Curie–Weiss law above this temperature.

Acknowledgments

The authors wish to thank M. Pernet for help and fruitful discussions.

References

[1] J.N. Reimers, J.E. Greedan, M.A. Subramanian, J. Solid State Chem. 79 (1989) 263.
[2] A.F. Wells, Structural Inorganic Chemistry, 5th Edition, Oxford University Press, Oxford, 1984.
[3] I.N. Belyaev, L.N. Averyanova, V.M. Erzhov, D.V. Balashov, Russ. J. Inorg. Chem. 17 (1972) 1490.
[4] M.A. Subramanian, A.W. Sleight, in: K.A. Gschneider, L. Eyring (Eds.), Handbook on the Physics and Chemistry of Rare Earths, Vol. 16, North-Holland, Amsterdam, 1993, p. 225.
[5] F. Brisse, D.J. Stewart, V. Seidl, O. Knop, Can. J. Chem. 50 (1972) 3648.
[6] B.M. Wanklyn, J. Crystal Growth 7 (1970) 368.
[7] S.H. Smith, B.M. Wanklyn, J. Crystal Growth 21 (1974) 23.
[8] D. Elwell, H.J. Scheel, Crystal Growth From High-Temperature Solutions, Academic Press, London, 1975.
[9] A.M. Nakua, J.E. Greedan, J. Crystal Growth 154 (1995) 334.
[10] P. Strobel, J.P. Lévy, J.C. Joubert, J. Solid State Chem. 66 (1984) 257.
[11] X.J. Yang, W.P. Tang, H. Kanoh, K. Ooi, J. Mater. Chem. 9 (1999) 2683.

[12] J. Akimoto, Y. Takahashi, Y. Gotoh, S. Mizuta, Chem. Mater. 12 (2000) 3246.
[13] M.E. Leonowicz, K.R. Poeppelmeier, J.M. Longo, J. Solid State Chem. 59 (1985) 71.
[14] C. Guého, P. Leone, P. Palvadeau, Comptes Rend. Acad. Sci. II 317 (1993) 595.
[15] Z. Otwinowski, C. Minor, in: C.W. Carter, R.M. Sweet (Eds.), Methods in Enzymology, Vol. 276, Academic Press, New York, 1997, pp. 307–326.
[16] S. Mackay, C.J. Gilmore, C. Edwards, N. Stewart, K. Shankland, MaXus Computer Program for the Solution and Refinement of Crystal Structures, Bruker Nonius, The Netherlands, 1999.
[17] P. Coppens, in: F.R. Ahmed, S.R. Hall, C.P. Huber (Eds.), Crystallographic Computing, Munksgaard, Copenhagen, 1970, pp. 255–270.
[18] A. Altomare, M.C. Burla, G. Camalli, G. Cascarano, C. Giacovazzo, A. Guagliardi, G.J. Polidori, J. Appl. Crystallogr. 27 (1994) 435–436.
[19] V. Petricek, M. Dusek, Institute of Physics, Academy of Sciences of the Czech Republic, Prague, 2000.
[20] P. Bordet, A. McHale, A. Santoro, R.S. Roth, J. Solid State Chem. 64 (1986) 30–46.
[21] J. Senegas, J. Galy, J. Solid State Chem. 10 (1974) 5–11.
[22] R.D. Shannon, Acta Crystallogr. A 32 (1976) 751.
[23] N.E. Brese, M. O'Keeffe, Acta Crystallogr. B 47 (1991) 192.